analytical chemistry

Article

pubs.acs.org/ac

On-Chip Colorimetric Detection of Cu^{2+} Ions via Density-Controlled Plasmonic Core–Satellites Nanoassembly

Hyeon Don Song,[†,§] Inhee Choi,[†,§,∥] Suseung Lee,[†] Young In Yang,[†] Taewook Kang,[‡] and Jongheop Yi*[,†]

[†]World Class University Program of Chemical Convergence for Energy and Environment, School of Chemical and Biological Engineering, Institute of Chemical Processes, Seoul National University, Seoul 151-742, Republic of Korea

[‡]Department of Chemical and Biomolecular Engineering, Sogang University, Seoul, 121-742, Republic of Korea

Supporting Information

ABSTRACT: We report on an on-chip colorimetric method for the detection and analysis of Cu^{2+} ions via the targeted assembly of plasmonic silver nanoparticles (2.6 nm satellites) on density-controlled plasmonic gold nanoparticles (50 nm cores) on a glass substrate. Without any ligand modification of the nanoparticles, by directly using an intrinsic moiety (carboxylate ion, COO^-) surrounded with nanoparticles, the method showed a high selectivity for Cu^{2+}, resulting in a nearly 2 times greater optical response compared to those of other metal ions via the targeted core–satellites assembly. By modulating the surface chemistry, it was possible to control the density of core gold nanoparticles on the surface, thus permitting easy tuning of the optical responses induced by plasmon coupling generated between each core–satellites nanostructure. Using chips with a controlled optimal core density, we observed the remarkable scattering color changes of the chips from green to yellow and finally to orange with the increase of Cu^{2+} concentration. The detection limits of the fabricated chips with controlled core densities (ca. 1821 and 3636 particles/100 μm^2) are 10 nM and 10 pM, respectively, which are quite tunable and below the level of 20 μM (or 1.3 ppm) defined by the United States Environmental Protection Agency. The findings suggest that the method is a potentially promising protocol for detecting small molecules with target selectivity and the tunability of the detection limits by replacing with ligands and adjusting core densities.

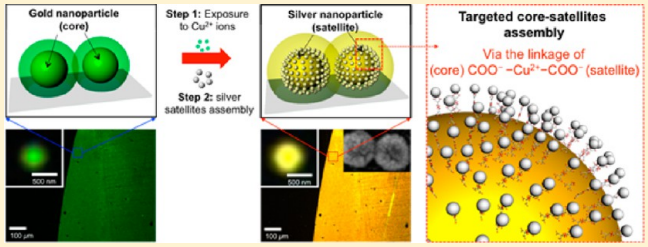

The detection of metal ions in aqueous solutions is great importance in terms of environmental protection and understanding ion cycling in biological systems. Among such ions, Cu^{2+} is an essential metal ion for biological functions (i.e., catalytic, biosynthetic, and transport processes within cells); however, it becomes toxic to the human body when uptake is excessive. To this regard, United States Environmental Protection Agency (EPA) defines the limit of Cu^{2+} ions in drinking water to be 20 μM (or 1.3 ppm). Therefore, the accurate detection of Cu^{2+} ions at the trace level in environmental and biological samples is a critical issue.

To achieve this, several methods for the detection of Cu^{2+} in aqueous solution have been developed, including not only atomic absorption spectroscopy,[1,2] voltammetry,[3,4] and inductively coupled plasma mass spectrometry[5,6] as classical detection methods, but also optical sensors based on surface plasmon resonance[7,8] and fluorescence.[9,10] Although most of methods have comparable sensitivity of under the EPA regulation level, their detection ranges are narrow (2–4 orders of magnitude, 10^2–10^4) except for inductive coupled plasma mass spectrometry (see Table S1 in the Supporting Information). Moreover, spectral analyses should be accompanied for the detection of Cu^{2+}.

As an alternative, the observation of light scattering from plasmonic nanoparticles can be an efficient method for developing a new sensing protocol due to their biocompatibility, photostability, and superior optical properties. In the case of plasmonic nanoparticles, plasmon couplings between them offer great opportunities for developing colorimetric sensing methods, since surface plasmon resonance generated by such couplings exhibits an extremely strong and distance-dependent spectral shifts (i.e., red-shift of an existing plasmon band and/or the formation of a new plasmon band). In this regard, colorimetric sensing methods based on the aggregation of nanoparticles in a colloidal solution have been extensively developed by utilizing ligand-modified nanoparticles with a target specificity. These solution-based colorimetric methods can be quite useful for detecting small molecules (e.g., oligonucleotides[11−15] and metal ions[16−20]); however, minor problems including undesirable aggregations induced by solution conditions (i.e., pH, temperature, and salt concentration) remain as an issue. This often occurs as the result of the self-aggregation of nanoparticles in a solution during the ligand modification process and the subsequent loss of a fraction of the nanoparticles. If it is possible to transfer nanoparticles from a colloidal solution to a solid substrate,

Received: June 16, 2013
Accepted: July 18, 2013
Published: July 18, 2013

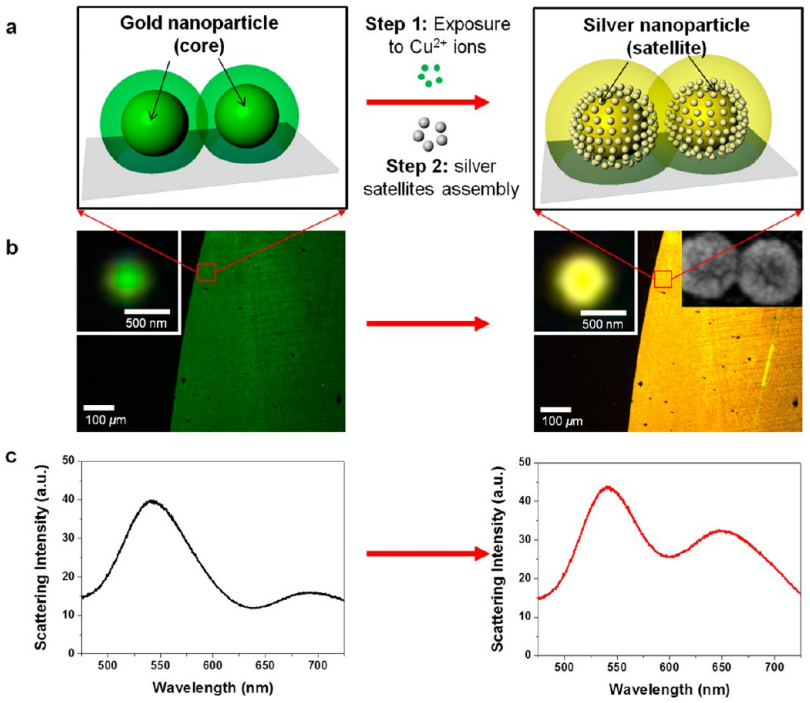

Figure 1. Schematic illustration of the on-chip colorimetric detection of Cu^{2+} ions via targeted core–satellites nanoassemblies. (a) Illustration of an interstructural plasmonic coupling between Cu^{2+} ion mediated plasmonic core–satellites structures. (b and c) Representative color and spectral changes after formation of Cu^{2+} ion medicated core–satellites structures. Scale bars are 500 nm and 100 μm, respectively.

these issues could be readily overcome. By utilizing surface-immobilized colloidal nanoparticles as plasmonic cores, it would be possible to carry out the postfunctionalization of core nanoparticles with target-specific ligands and/or the further assembly of other satellite nanoparticles around them, which would successfully minimize undesirable nanoparticle aggregation unlike the case of a solution. Such targeted assemblies of foreign plasmonic nanoparticles around the immobilized core nanoparticles, that is core–satellites assemblies, result in distinct and measurable plasmonic shifts that occur as a function of changes in the dielectric properties around the core nanoparticles. We recently reported that these core–satellites assemblies can be employed as a sensing principle by systemically showing the changes in Rayleigh light scattering spectra measured for individual single core gold nanoparticles with increasing number of satellite particles.[21] From this finding, we hypothesized that the plasmon couplings generated from a single core–satellites assembly would be enhanced through the high-density immobilization of core particles on the surface, thus allowing significant plasmonic couplings between core–satellites nanostructures.

In the present study, we report on the further development of an on-chip colorimetric method for the detection and measurement of Cu^{2+} ions via targeted assembly between plasmonic gold nanoparticles (cores) and plasmonic silver nanoparticles (satellites). We directly utilized an intrinsic moiety (carboxylate ion, COO^-) surrounded with nanoparticles to induce a Cu^{2+} mediated core–satellite assembly without any further ligand modification of nanoparticles. In addition, it was possible to control the density of core gold nanoparticles on the surface for maximizing the optical responses induced by the plasmon coupling generated from the targeted silver satellites assemblies. The strategy also has promise for use in detecting other small molecules by replacing with target-specific ligands and adjusting core density.

RESULTS AND DISCUSSION

The underlying concept of the system for detecting Cu^{2+} ions is illustrated in Figure 1a. The coupling between plasmonic structures mainly depends on their intrinsic plasmonic properties (usually determined by the shape and size of the structure) and interstructural distances. Therefore, we hypothesized that interstructural coupling among core–satellites structures as well as interparticle coupling between a core and satellites would occur, which provides enormous signal enhancements. In addition, the carboxylate ion (COO^-), as an intrinsic moiety surrounded with nanoparticles, was directly utilized to induce the targeted assembly of nanoparticles without any need for the functionalization of nanoparticles since the COO^- group has a high affinity for Cu^{2+}. Note that the synthesis of nanoparticles normally involves stabilization with a reducing agent (e.g., in our case, citric acid with COO^-).[22,23]

The sensor chips were fabricated by the immobilization of 50 nm gold nanoparticles as core particles. The distance between the core gold nanoparticles can be controlled by simple wet chemistry based on our previously reported protocol (a stepwise mixed self-assembled monolayer preparation method[24]). The fabricated chip was characterized by dark-field microscopy combined with a true color imaging camera and a spectrometer (see the Experimental Methods section and Figure S1 in the Supporting Information). Briefly, a particle is illuminated with the white light of a dark-field microscope in the transmission mode, and an image and a profile of the Rayleigh scattered light are then collected by the camera and the spectrometer, respectively. In our typical experiments, a core–satellites assembly composed of core gold nanoparticles

dx.doi.org/10.1021/ac401796q | Anal. Chem. 2013, 85, 7980–7986

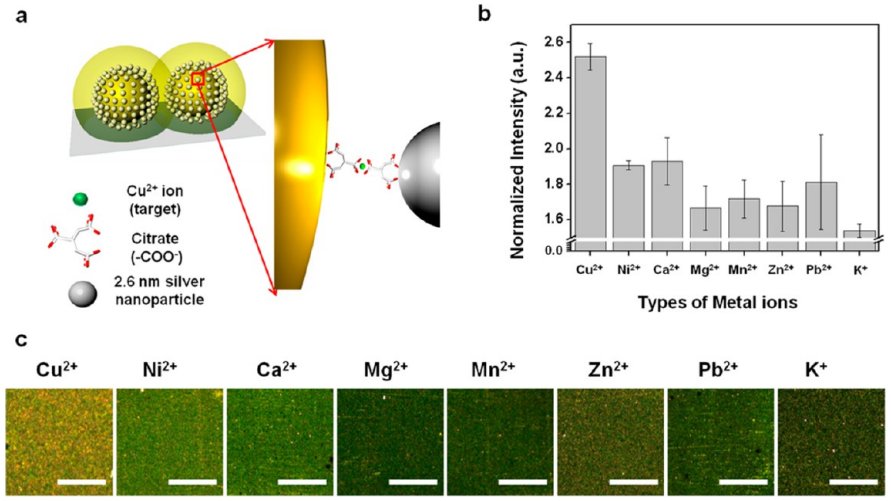

Figure 2. Cu^{2+} selective colorimetric responses induced by the formation of core−satellites nanostructures. (a) The Cu^{2+} mediated core−satellites assembly induced by the formation COO^-−Cu^{2+}−COO^- linkage. (b and c) Change in scattering intensities for a longer plasmon band (around 675 nm) and scattering images after core−satellites assemblies induced by various metal ions at an identical concentration of 100 nM. The observed remarkable difference in the scattering intensities is due to the differential affinity between COO^- and metal ion species. Scale bar is 100 μm.

(50 nm in diameter) linked by metal ions to satellite silver nanoparticles (2.6 nm in diameter) was used for the following reasons. First, the synthesis of nanoparticles usually involves stabilization with a reducing agent, in our case a citric acid with carboxylate (COO^-) moieties, which have a high affinity to metal ions by virtue of the fact that they form metal−carboxylate complexes.[25] Thus, our approach does not involve the complicated surface modification of nanoparticles, which results in a significant simplification in the satellite assembly. Second, a 50 nm gold nanoparticle, as a core, provides an excellent platform with multiple coordination sites for metal ions (e.g., a 50 nm gold particle can tether approximately 640 ± 80 thiolated ligands on its surface[26]), which could lead to an assembly of high-density satellites. Last, as satellites, 2.6 nm silver nanoparticles perform an excellent role in inducing tunable plasmon coupling, which occurs as a function of the amount of the complexed target metal ions, because they are sufficiently small that their binding to the core can be directly correlated with the amount of target metal ions absorbed onto the core nanoparticles. Parts b and c of Figure 1 show typical characteristics for our approach. A color change from green to yellow induced by the Cu^{2+} ion mediated core−satellites assemblies was clearly observed (Figure 1b). This color change is also correlated with the spectral change (Figure 1c) showing the generation of a plasmon band at a longer wavelength.

On the basis of the proposed sensing principle, we first examined the selectivity of the system for Cu^{2+}, which is determined by the affinity of binding between COO^- and the metal ion species (Figure 2a). We tested eight environmentally and biologically relevant metal ions (Cu^{2+}, Ni^{2+}, Ca^{2+}, Mg^{2+}, Mn^{2+}, Zn^{2+}, Pb^{2+}, and K^+) at an identical concentration of 100 nM. The bar graph (Figure 2b) and dark-field images (Figure 2c) summarize the differential responses for the different metal ions. Among the metal ions tested, Cu^{2+} ions induced the most dramatic change in scattering intensity (Figure 2b and Figure S2 in the Supporting Information) and scattering color (Figure 2c) after the core−satellites assemblies. This can be attributed to the strong affinity between COO^- and Cu^{2+}, compared to other metal ions.[21,25] It should be noted that the difference in optical responses for divalent metal ions (i.e., $Cu^{2+} \gg Ni^{2+}$, $Ca^{2+} > Mn^{2+}$, Mg^{2+}) is well-consistent with the order of binding strength between citric acids and the metal ions.[25] Morcellet also reported that the formation of a chelated complex between carboxyl groups and various metal ions involves different enthalpies with the following order of ΔH ($Cu^{2+} > Zn^{2+} > Cd^{2+} > Ni^{2+} > Mn^{2+} > Mg^{2+}$).[27] At an identical concentration of 100 nM, the Cu^{2+} ion mediated assemblies of silver nanoparticles on core gold nanoparticles resulted in a nearly 2 times greater increase in the scattering intensity of a newly formed longer plasmon band, compared to the intensity of other metal ions (Figure S2 in the Supporting Information). This difference induces a color change to yellow in the case of Cu^{2+} ion (Figure 2c) while the color remains green for other metal ions. Thus, a much higher selectivity for Cu^{2+} ion is observed in the case of this proposed targeted core−satellites assembly.

To clearly demonstrate our sensing concept, we also measured a spectrum for the gold core particle treated with silver satellites nanoparticles, which has not been exposed to metal ions (i.e., without Cu^{2+}). In this case, no significant change in the spectrum (red graph of Figure S3a in the Supporting Information) indicating the nonformation of core−satellites nanoassembly was observed compared to Cu^{2+} mediated core (gold)−satellites (silver) assembly (blue graph of Figure S3a in the Supporting Information). Corresponding dark-field scattering images (Figure S3b in the Supporting Information) show a clear contrast for assembly and non-assembly for core−satellites structures.

Having shown that unmodified gold and silver plasmonic nanoparticles in themselves without ligand exchange have a comparable selectivity for Cu^{2+} ions, we next determined the optimal conditions for the method by tuning the density of core gold nanoparticles on a glass substrate for producing the maximal colorimetric response. The density of the core gold nanoparticle on the surface can be easily controlled by the time used for the immobilization of 3-aminopropyltriethoxysilane (APTES, $-NH_2$) and the subsequent octadecytrichlorosilane (OTS, $-CH_3$) treatment in the process of the stepwise formation of the mixed self-assembled monolayer.[24] Figure 3 provides information on the difference in scattering color change as a function of the initial density of core gold

dx.doi.org/10.1021/ac401796q | Anal. Chem. 2013, 85, 7980−7986

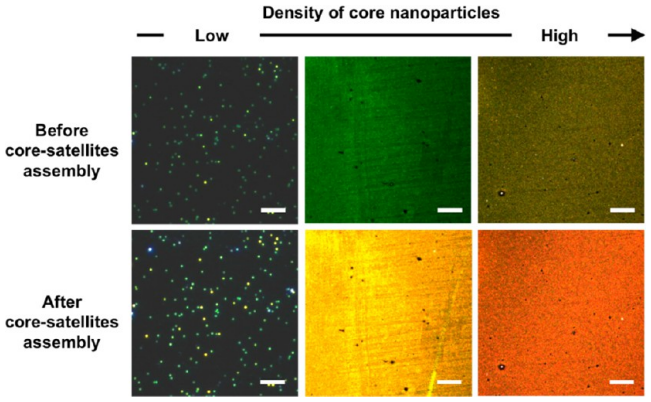

Figure 3. Difference in scattering color changes dependent on the initial density of core gold nanoparticles after the formation of core–satellites nanostructures. A 100 μM Cu^{2+} ion solution was exposed to core gold nanoparticles followed the formation of targeted assemblies of silver satellites nanoparticles. The density of core gold nanoparticles can be controlled by the stepwise formation of the mixed self-assembled monolayers composed of APTES ($-NH_2$) and OTS ($-CH_3$) under different preparation protocols. Left: individual core gold nanoparticles (cores are sparsely dispersed and no plasmon coupling between cores is shown); 10 min APTES treatment followed by a 3 h OTS treatment. Scale bar is 10 μm. Middle: medium density of core gold nanoparticles (cores are densely assembled but no plasmon coupling between cores occurs); 10 min APTES treatment followed by a 30 min OTS treatment. Scale bar is 100 μm. Right: high density of core gold nanoparticles (cores are very densely assembled and plasmon coupling between cores occurs); 30 min APTES treatment followed by a 20 min OTS treatment. Scale bar is 100 μm.

nanoparticles after a core–satellites assembly for 100 μM Cu^{2+}. When the surface immobilization of the nanoparticle is sufficiently sparse (left case of Figure 3: ca. 178 particles/100 μm^2, as determined from a scanning electron micrograph, see also Figure 4a) to resolve the single nanoparticles via dark-field scattering imaging, the scattering colors of individual nanoparticles become bright after the formation of a core–satellites assembly, as was confirmed in our previous study.[21] Adjusting the surface chemistry (i.e., a 10 min APTES treatment and followed by a 30 min OTS treatment) allowed the preparation of more densely assembled gold core nanoparticles (middle case of Figure 3). The color of the chip was perfectly green, which indicates that core gold nanoparticles are densely assembled compared to the previous case but no plasmon coupling between the cores occurs. In this case, the color is clearly changed to yellow after the formation of Cu^{2+} mediated core–satellites assemblies. By increasing the number of core nanoparticles per unit area by 10 times (right case of Figure 3: ca. 1821 particles/100 μm^2, see also Figure 4b), the initial color of the chip is tuned to yellowish green due to the plasmon coupling between core gold nanoparticles. It is noteworthy that the color of the fabricated chip dramatically changes to orange, after the formation of Cu^{2+} mediated core–satellites assembly. This can be attributed to the generation of interstructural coupling between the assembled core–satellites structures as the result of the decrease of interparticle distances between initial core gold nanoparticles. Scanning electron micrographs clearly show the difference in the density of core gold nanoparticles and their interparticle distances (Figure 4).

On the basis of these findings, we further controlled the distribution of core gold nanoparticles at high levels of densities, as summarized in Figure 4, parts b and c, and Table 1.

Table 1. Relative Densities of Core Nanoparticles and the Fabrication Protocol for Each Chip

relative particle density	low (Figure 4a)	high (Figure 4b)	very high (Figure 4c)
particle number (per 100 μm^2)	178	1821	3636
averaged interparticle distance (nm)	489	234	89
APTES treatment (min)	10	10	30
OTS treatment (min)	180	20	20

Using these fabricated chips with controlled high core densities (ca. 1821 and 3636 particles/100 μm^2), we investigated the detection limits of the fabricated chips. As the concentration of Cu^{2+} ions increases, the number of yellow and orange scattering spots (in lower magnified images of Figure 5, parts a and b) increases ultimately shifting the color of the chip from green (absence of Cu^{2+} ions) to yellow or orange (presence of Cu^{2+} ions). When the density of the preimmobilized core gold nanoparticles is approximately 1821 particles/100 μm^2, the color of the chip changes abruptly to an orange color at 100 μM and the detection limit was determined to be 10 nM (Figure 5a). When the density of core particles on the chip increases by a factor of 2 times (ca. 3636 particles/100 μm^2), the abrupt color change occurs at 100 pM and the detection limit is 10 pM or less (Figure 5b), which is at least 3 orders of magnitude lower than that of the previous case. This observation also provides a demonstration of the tunability of the proposed method. The spectral changes (Figure 5, parts c and e) are consistent with the observed concentration-dependent color changes induced by the Cu^{2+} ion mediated core–satellites assembly for both cases of the core densities. The shorter plasmon band is red-shifted slightly, and the newly

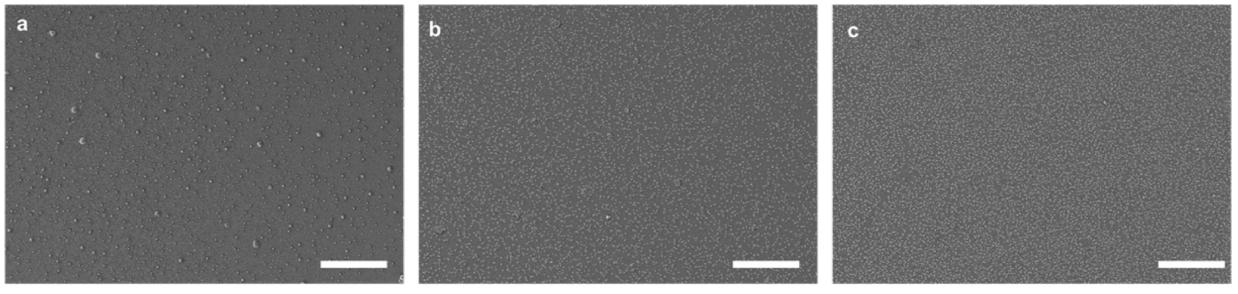

Figure 4. Scanning electron micrographs of the density-controlled chip surfaces: (a) ca. 178, (b) ca. 1821, and (c) ca. 3636 particles/100 μm^2. Scale bar is 5 μm.

dx.doi.org/10.1021/ac401796q | Anal. Chem. 2013, 85, 7980–7986

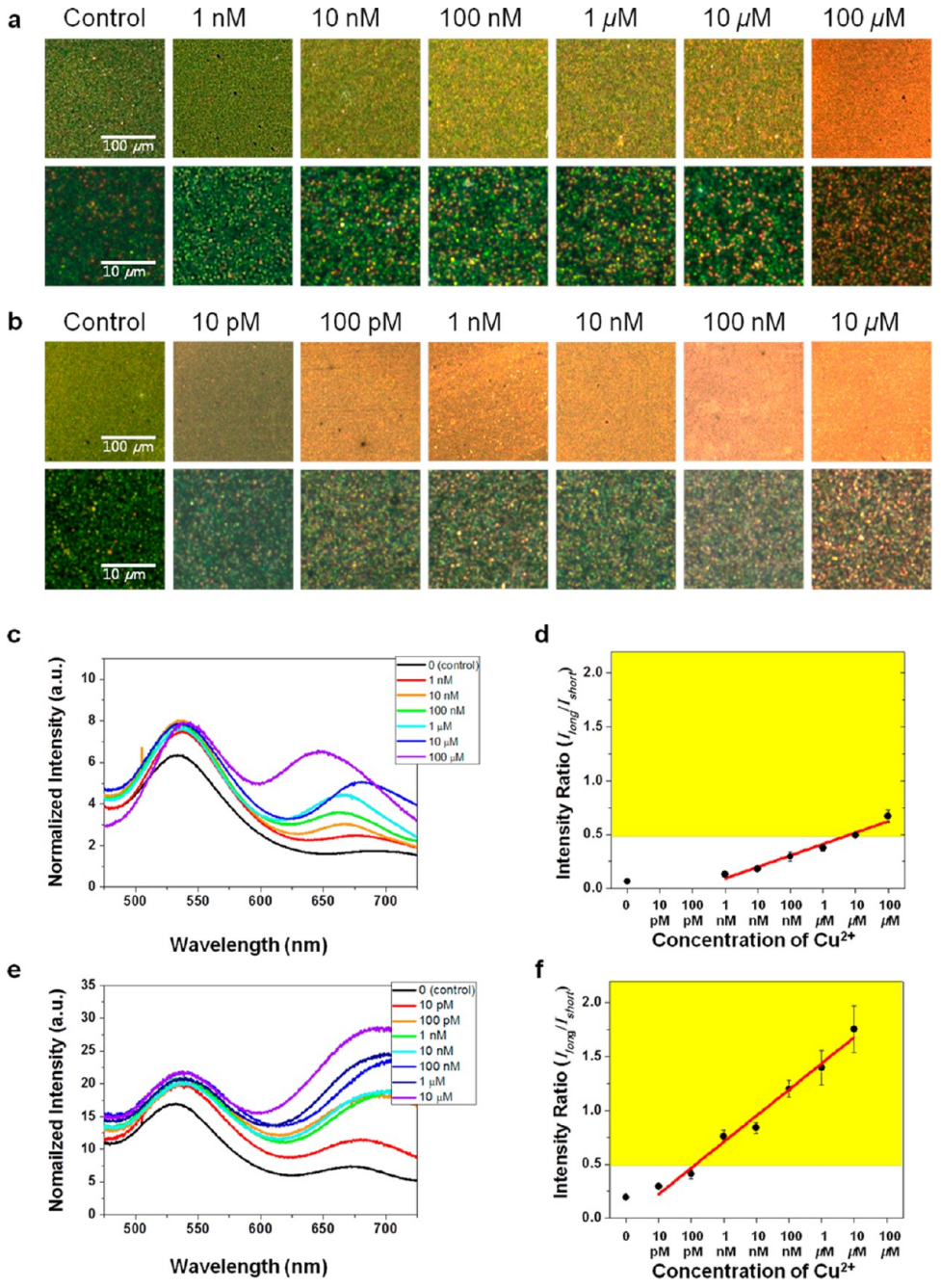

Figure 5. Cu^{2+} ion concentration-dependent colorimetric responses and the tunability of detection limits by controlling core nanoparticle densities. (a) Concentration-dependent dark-field scattering images when the density of preimmobilized core gold nanoparticles is approximately 1821 particles/100 μm^2. The color of the chip changes abruptly to an orange color at 100 μM, and the detection limit is 10 nM. The lower panel shows magnified images of the upper panel. (b) Concentration-dependent dark-field scattering images when the density of the core particles on the chip is 3636 particles/100 μm^2; the abrupt color change occurs at 100 pM, and the detection limit is 10 pM or less. The lower panel shows magnified images of the upper panel. (c and d) Corresponding scattering spectra and scattering intensity ratios at each Cu^{2+} concentration of panel a. (e and f) Corresponding scattering spectra and scattering intensity ratios at each Cu^{2+} concentration of panel b. Plots depicting ratios of the scattering intensities between the short plasmon band (around 550 nm) and the long plasmon band (around 675 nm) show linear displacements for the increase in Cu^{2+} concentration in both cases (panels d and f). Error bars are included on all data points. The red lines are logarithmic fits to the Cu^{2+} concentration. The regression coefficient (R^2) is 0.9718 (panel d) and 0.9733 (panel f), respectively.

formed longer plasmon band increases with increasing Cu^{2+} concentration. It should be noted that the existence of the weak longer plasmon band in the initial chip in the case of high density of core particles (in a black graph of Figure 5e) is due to plasmon coupling between core gold nanoparticles. As a result, the increase in the scattering intensities at a longer wavelength (Figure 5e) is much greater than that of the lower density of core particles (Figure 5c), in accordance with the increase in Cu^{2+} concentration. Plots depicting the ratios of the intensities between the short plasmon band (around 550 nm) and the long plasmon band (around 675 nm) show linear displacements for the increase in Cu^{2+} concentration in both cases (Figure 5, parts d and f). Our proposed method shows a substantial dynamic detection range over 5−6 orders of

dx.doi.org/10.1021/ac401796q | Anal. Chem. 2013, 85, 7980−7986

magnitude. By correlating with the obtained images, the color change to orange can be attributed to an increase in the intensity ratio over 0.4−0.5 (marked with yellow boxes). Moreover, the ratios of the red to green, obtained from RGB analyses of the dark-field images, are likewise consistent with the concentration-dependent linear relationship (Figure S4 in the Supporting Information). This provides an additional support for the feasibility of the proposed method. Consequently, our results show an excellent linearity at levels well below the level of 20 μM (or 1.3 ppm) defined by the EPA. The method described in this study is sufficiently sensitive to detect Cu^{2+} in an aqueous media and allows Cu^{2+} to be detected at the picomolar level, which is a considerable reduction in the detection limit compared to the currently used conventional optical methods.

CONCLUSIONS

In summary, a picomolar level on-chip colorimetric detection method of Cu^{2+} ions was developed. The basic principles of the method involve the targeted assembly of plasmonic silver nanoparticles (satellites) onto plasmonic gold nanoparticles (cores) immobilized on a glass substrate. Without any ligand modification of nanoparticles, we successfully achieved a high selectivity for Cu^{2+}, resulting in a nearly 2 times greater optical response compared to the corresponding responses of other metal ions via the formation of a targeted core−satellites assembly. In addition, controlling the density of core gold nanoparticles on the detection chip allowed one to easily tune the optical responses stemming from plasmon couplings between core−satellites structures. As a result, a detection limit and a dynamic range are adjustable. Using the fabricated chips with controlled optimal core densities, we observed remarkable scattering color changes of the chips from green to yellow and finally to orange as a function of increasing Cu^{2+} concentration. The detection limit of the fabricated chips with controlled core densities is below 10 pM, which is a much lower level than the regulation value of 20 μM (or 1.3 ppm) defined by the U.S. EPA.

In conclusion, our method is sufficiently sensitive to permit the detection of Cu^{2+} in an aqueous media and allows Cu^{2+} to be detected at the picomolar level or lower, which is a considerable reduction in the detection limit compared to the conventional metal ion detection methods. Moreover, the proposed method can be extended to the detection of biologically and environmentally relevant analytes by using desirable molecular recognition motifs (e.g., metal chelating moiety/metal ions, metalloprotein/metal ions, biotin/streptavidin, antibody/antigen, and complementary oligonuleotides). In addition, our method has several key advantages: (1) A detection limit and a dynamic range are adjustable to a level of the concentration of interest for a target analyte. (2) The sensing principle is favorable to develop a multiplexed detection platform owing to the differential optical properties depending on the shape, size, and composition of plasmonic nanoparticles. (3) The developed sensing chip is highly feasible to assemble into a fully integrated optofluidic monitoring system. Collectively, our method represents a promising method for efficiently detecting small molecules in terms of the selectivity, the tunability of detection limits, and the capabilities of multiplexing and system integration.

EXPERIMENTAL METHODS

Materials. Gold nanoparticles (50 nm in diameter) were purchased from BBI International, Inc. 3-Aminopropyltriethoxysilane and octadecyltrichlorosilane were purchased from Sigma-Aldrich. Copper sulfate ($CuSO_4$) and other metal salts were purchased from Sigma-Aldrich. Silver nitrate ($AgNO_3$), sodium borohydride ($NaBH_4$), sodium citrate dehydrate ($Na_3C_6H_5O_7 + 2H_2O$), and poly(vinylpyrrolidone) (PVP) were purchased from Sigma-Aldrich. All water used was purified to above 18 MΩ using a Milli-Q DI water system (Millipore).

Preparation of 2.6 nm Silver Nanoparticles. Silver nanoparticles (diameter, 2.6 nm) were synthesized by a previously reported protocol.[21] Briefly, $AgNO_3$ (0.11 mM), sodium citrate (1.91 mM), PVP (0.052 mM), and H_2O_2 (25.0 mM) in 42.3 mL of DI water were mixed and stirred constantly. As $NaBH_4$ (150 μL, 100 mM) was added to the mixture, the color of the solution turned to light yellow. After stirring for an additional 3 h, the solution was filtered using 0.2 μm membrane filters.

Density Control of Single Gold Nanoparticles on a Glass Slide. Prior to the immobilization of single gold nanoparticles, glass slides were cleaned in a piranha solution (H_2SO_4/H_2O_2 = 7:3 v/v) for 1 h, followed by rinsing with DI water and drying in a stream of N_2. A cleaned glass slide was immersed in an ethanolic solution of 5 mM APTES and incubated for 10 min periods (i.e., 10 min and 30 min, to control the surface density of amine moieties occupied by gold nanoparticles). The modified surface with APTES was sonicated in pure ethanol to remove excess reagents, followed by drying in a stream of N_2. The remaining area (unoccupied by APTES) on the glass slide was then passivated by treatment for different periods of time with a 5 mM OTS in a toluene solution for different times (i.e., 3 h, 30 min, and 20 min, to control the interparticle distance). For the immobilization of single gold nanoparticles, 200 μL of a colloidal solution containing 50 nm diameter gold nanoparticles was dropped onto the modified glass slide. After 10 min, the physically deposited gold nanoparticles were washed with DI water and the glass slide was dried in a stream of N_2.

Formation of Cu^{2+} Ion Mediated Core−Satellites Structures. For the formation of Cu^{2+} ion mediated core−satellites structures, various concentrations of Cu^{2+} solutions were dropped onto the gold nanoparticles immobilized on the glass slide. After 1 h, the glass slide was washed with DI water and dried in a stream of N_2. The prepared 2.6 nm silver nanoparticles solution was then dropped onto the Cu^{2+} treated gold nanoparticles immobilized on the glass slide. After 3 h, the core−satellite structures immobilized on a glass slide were washed with DI water and dried in a stream of N_2. In order to validate a higher selectivity for Cu^{2+} in the formation of core−satellites structure, compared to other metal ions, control experiments were also performed for several cases (i.e., only silver nanoparticles treatment without exposure to Cu^{2+}, and other metal ion solutions, such as Ni^{2+}, Ca^{2+}, Mg^{2+}, Mn^{2+}, Zn^{2+}, Pb^{2+}, and K^+).

Dark-Field Imaging and Measuring Scattering Spectra of the Assembled Core−Satellites Structures. The dark-field microscopy system for imaging and measuring spectra of the chip consisted of an Axio Observer Z1 inverted microscope (Carl Zeiss, Germany) equipped with a dark-field condenser (numerical aperture = 0.8−1.4), a true-color digital camera, and a 1024 pixel × 256 pixel cooled spectrograph CCD camera

dx.doi.org/10.1021/ac401796q | Anal. Chem. 2013, 85, 7980−7986

(Andor Technology PLC, U.K.). Illumination was provided by an integrated 100 W halogen source. A two-way adapter with a selectable output was connected to the camera port of the microscope. This allows the sample image to be directed to either a color digital camera or a line-imaging spectrometer. The spectrophotometer (Monora320i, Dongwoo Optron Co., Korea), with a grating of 300 grooves mm^{-1} was used to collect spectra from the chip. For all spectral data, the reliability of the measured spectral shift and intensity ratio (I_{LONG}/I_{SHORT}) were examined by the standard deviation of the spectral shift from five different positions on the chip.

■ ASSOCIATED CONTENT

Supporting Information

A table summarizing detection limits and ranges of previous methods and experimental data including configuration of the dark-field microscope system, representative spectral changes for various metal ions after core−satellites assembly, optical responses for the substrate treated without Cu^{2+}, and RGB analyses for dark-field images. This material is available free of charge via the Internet at http://pubs.acs.org.

■ AUTHOR INFORMATION

Corresponding Author

*E-mail: jyi@snu.ac.kr. Phone: +82-2-880-7438.

Present Address

[‖]Department of Bioengineering, University of California at Berkeley, Berkeley, California 94720, United States.

Author Contributions

[§]H.D.S. and I.C. contributed equally to this work.

Notes

The authors declare no competing financial interests.

■ ACKNOWLEDGMENTS

This work was supported by Grant No. 101-081-032 from the Ministry of Environment, Korea, and the WCU (World Class University) program through the National Research Foundation of Korea funded by the Ministry of Education, Science and Technology (R31-10013). It was also supported by the National Research Foundation of Korea (NRF) grant funded by the Korea government (MEST) (No. 2011-0015749).

■ REFERENCES

(1) Harnly, J. M. *J. Anal. At. Spectrom.* **1999**, *14*, 137−146.
(2) Demirbas, A.; Pehlivan, E.; Gode, F.; Altun, T.; Arslan, G. *J. Colloid Interface Sci.* **2005**, *282*, 20−25.
(3) Baldo, M. A.; Daniele, S.; Ciani, I.; Bragato, C.; Wang, J. *Electroanalysis* **2004**, *16*, 360−366.
(4) Osipova, E. A.; Sladkov, V. E.; Kamenev, A. I.; Shkinev, V. M.; Geckeler, K. E. *Anal. Chim. Acta* **2000**, *404*, 231−240.
(5) Hutton, R. C. *J. Anal. At. Spectrom.* **1986**, *1*, 259−263.
(6) Karami, H.; Mousavi, M. F.; Yamini, Y.; Shamsipur, M. *Anal. Chim. Acta* **2004**, *509*, 89−94.
(7) Forzani, E. S.; Zhang, H. Q.; Chen, W.; Tao, N. J. *Environ. Sci. Technol.* **2005**, *39*, 1257−1262.
(8) Kang, T.; Hong, S. R.; Moon, J.; Oh, S.; Yi, J. *Chem. Commun.* **2005**, 3721−3723.
(9) Prestel, H.; Gahr, A.; Niessner, R. *Fresenius' J. Anal. Chem.* **2000**, *368*, 182−191.
(10) Xiang, Y.; Tong, A. J.; Jin, P. Y.; Ju, Y. *Org. Lett.* **2006**, *8*, 2863−2866.
(11) Elghanian, R.; Storhoff, J. J.; Mucic, R. C.; Letsinger, R. L.; Mirkin, C. A. *Science* **1997**, *277*, 1078−1081.
(12) Li, H. X.; Rothberg, L. *Proc. Natl. Acad. Sci. U.S.A.* **2004**, *101*, 14036−14039.
(13) Reynolds, R. A.; Mirkin, C. A.; Letsinger, R. L. *Pure Appl. Chem.* **2000**, *72*, 229−235.
(14) Jin, R. C.; Wu, G. S.; Li, Z.; Mirkin, C. A.; Schatz, G. C. *J. Am. Chem. Soc.* **2003**, *125*, 1643−1654.
(15) Cao, Y. C.; Jin, R. C.; Thaxton, S.; Mirkin, C. A. *Talanta* **2005**, *67*, 449−455.
(16) Lee, J. S.; Han, M. S.; Mirkin, C. A. *Angew. Chem., Int. Ed.* **2007**, *46*, 4093−4096.
(17) Kim, Y. J.; Johnson, R. C.; Hupp, J. T. *Nano Lett.* **2001**, *1*, 165−167.
(18) Xu, X. W.; Wang, J.; Jiao, K.; Yang, X. R. *Biosens. Bioelectron.* **2009**, *24*, 3153−3158.
(19) Alizadeh, A.; Khodaei, M. M.; Karami, C.; Workentin, M. S.; Shamsipur, M.; Sadeghi, M. *Nanotechnology* **2010**, *21*, 315503.
(20) Yang, Y. I.; Choi, I.; Hong, S.; Lee, S.; Kang, T.; Lee, H.; Yi, J. *J. Nanosci. Nanotechnol.* **2010**, *10*, 3538−3542.
(21) Choi, I.; Song, H. D.; Lee, S.; Yang, Y. I.; Kang, T.; Yi, J. *J. Am. Chem. Soc.* **2012**, *134*, 12083−12090.
(22) Chah, S.; Hutter, E.; Roy, D.; Fendler, J. H.; Yi, J. *Chem. Phys.* **2001**, *272*, 127−136.
(23) Huang, T.; Nallathamby, P. D.; Xu, X. H. N. *J. Am. Chem. Soc.* **2008**, *130*, 17095−17105.
(24) Choi, I.; Kim, Y.; Kang, S. K.; Lee, J.; Yi, J. *Langmuir* **2006**, *22*, 4885−4889.
(25) Mengel, K. *Principles of Plant Nutrition*, 5th ed.; Kluwer Academic Publishers: Dordrecht, The Netherlands; Boston, MA, 2001.
(26) Hill, H. D.; Millstone, J. E.; Banholzer, M. J.; Mirkin, C. A. *ACS Nano* **2009**, *3*, 418−424.
(27) Morcellet, M. *Polym. Bull.* **1984**, *12*, 127−132.